Journal of the Korean Physical Society, Vol. 56, No. 1, January 2010, pp. 309∼314

X-ray Radiation Emitted from the Betatron Oscillation of Electrons in Laser Wakefields

Seok Won Hwang and Hae June Lee*
Department of Electrical Engineering, Pusan National University, Busan 609-735

Sang Young Chung and Dong-Eon Kim
Department of Physics,
Pohang University of Science and Technology, Pohang 790-784

(Received 16 January 2009)

An ultra-intense short laser pulse incident on a plasma generates a blowout-regime wakefield, where almost all of the electrons are expelled radially by the ponderomotive force. Electrons injected in an off-axis position of the blowout-regime wakefield experience transverse oscillations as well as longitudinal acceleration, and emit intense X-rays from betatron oscillations. In order to investigate the conditions for X-ray generation, we simulated the relativistic electron motion from wakefield profiles pre-calculated with a two-dimensional particle-in-cell code. The maximum energy of the off-axis injected electrons reaches 900 MeV for a propagation time of 20 ps and the electron emits intense X-ray radiation with energies up to 13 keV.

PACS numbers: 52.38.Kd, 52.38.Ph, 52.38-r
Keywords: X-ray generation, Betatron oscillation, Laser wakefield, Electron acceleration
DOI: 10.3938/jkps.56.309

I. INTRODUCTION

After the invention of ultra-high intensity lasers, particle acceleration techniques using laser wakefields have developed rapidly [1]. Laser-induced particle accelerators can have an acceleration gradient of 10 – 100 GV/m, which is higher by three orders of magnitude than that of conventional linear accelerators [2]. The normalized electric field intensity of the laser pulse is defined as

$$a = \frac{eE}{mc\omega}, \tag{1}$$

where e, m, c, ω, and E are the elementary charge, the electron mass, the speed of light, the laser frequency, and the electric field intensity, respectively. If a is higher than 1.0, the wakefields start to form blowout regions. In the blowout regime, all of plasma electrons are expelled from the laser propagation axis, and intense electric fields higher than those in linear regime are generated. Recently, Lu *et al.* [3, 4] reported a theory for nonlinear, multidimensional plasma wakefields in the blowout regime. No transverse change of acceleration fields is shown, which helps to prevent the electrons from spreading.

The accelerated electron beam experiences a radial restoring force generated by the space charge effect of the background ions, and it undergoes betatron oscillations. Since 2002, the oscillation has been reported to give rise to the emission of intense femtosecond X-ray radiation over a few keV. The betatron X-ray was observed using a 28.5-GeV electron beam, and it was verified that the plasma could be used as a wiggler in a free electron laser [5]. A three-dimensional particle-in-cell simulation was conducted with a bunch of 25-GeV electron beam [6]. It was shown that a keV X-ray beam could be generated by simply focusing a single high-intensity laser pulse into a gas jet [7]. From the images of betatron radiation of the electrons in the wakefields [8], the electron trajectories could be estimated. Accurate measurements of the X-ray spectra were used to characterize the initial amplitude of the betatron osicllation [9]. A recent experiment reported that a petawatt-laser-generated plasma cavity produced 50-keV X-ray beams [10].

In this paper, we present an analysis of the single electron motion in the blowout regime using a two-dimensional particle-in-cell code. For the sake of a simple analysis, we assumed that the wakefield did not vary during the electron acceleration time. Section II demonstrates the simulation method and the characteristics of the generated blowout regime. In Section III, the single electron motion is demonstrated for particles located in the accelerating and focusing blowout regimes. The radiation spectrum from the single electron motion is ana-

*E-mail: haejune@pusan.ac.kr; Fax: +82-51-510-1498

lyzed at various transverse injection positions. The time evolution of the radiation is demonstrated, and the radiation spectrum from a mono-energetic electron bunch is presented. The conclusion and discussions are presented in Section IV.

II. SIMULATION METHOD

1. Parameters for Wakefield Generation

For the investigation of X-ray emission from betatron oscillations, a two-dimensional electromagnetic particle-in-cell code (XOOPIC) [11] was utilized. The simulation was conducted in z-x rectangular coordinates. The simulation parameters are similar to those reported in Ref. 4. The size of the simulation domain is 96 μm in the z direction and 96 μm in the x direction. The grid size was chosen to be $\Delta z = \Delta x = \lambda/16$, where λ is the wavelength of the laser. The electron plasma density is $n_0 = 1.93 \times 10^{18}$ cm^{-2}. The incident laser pulse has a Gaussian distribution with a full width at half maximum (FWHM) of 30 fs. The waist of the laser was chosen to be a large value, 19.5 μm, to increase the strength parameter K, which is defined as

$$K = 1.33 \times 10^{-10} \gamma^{1/2} n_e^{1/2} [\mathrm{cm}^{-3}] r_0 [\mu\mathrm{m}] \ , \qquad (2)$$

where n_e is the electron density, γ is the relativistic factor, and r_0 is the amplitude of the betatron oscillation. The characteristics of the radiation depend strongly on r_0, and the radiation is emitted in the forward direction within a cone angle of K/γ [7].

The peak amplitude of the normalized vector potential, a_0, is related to the peak intensity I by

$$a_0 = 8.5 \times 10^{-10} \lambda [\mu\mathrm{m}] I^{1/2} [\mathrm{W/cm}^2] \ . \qquad (3)$$

The intensity of the laser pulse used in this simulation is 3.46×10^{19} W/cm^2 which corresponds to $a_0 = 4.0$ with $\lambda = 800$ nm.

2. Wakefield Profiles

When an ultra-intense laser pulse propagates into a plasma, most of electrons are expelled by the radiation pressure, and blowout regimes occur. Figure 1 shows the profiles of the electron density of the wakefields generated using the parameters stated above. The blowout radius R is estimated to be about 17 μm, which is a little less than the waist size of the laser. The peak density of the electrons in the wakefield is 2.474×10^{19} cm^{-3}, which is 12.8 times larger than the uniform plasma density n_0.

A strong space charge separation induces intense electric fields. Figure 2 shows the cross-sectional profiles of the longitudinal and the transverse electric fields, E_z and

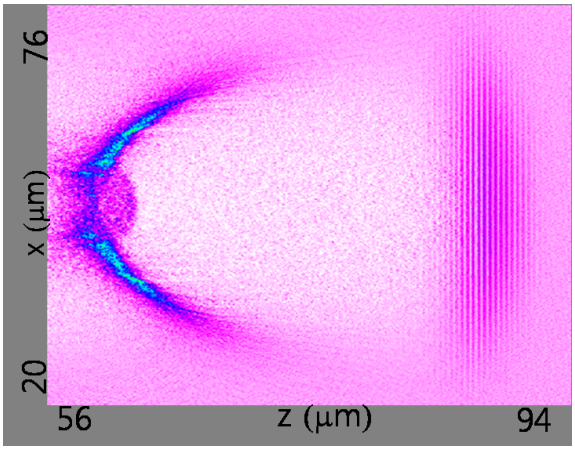

Fig. 1. (Color online) The electron density profile is shown near a position behind the laser pulse. The peak density (blue) reaches 2.474×10^{19} cm^{-3}.

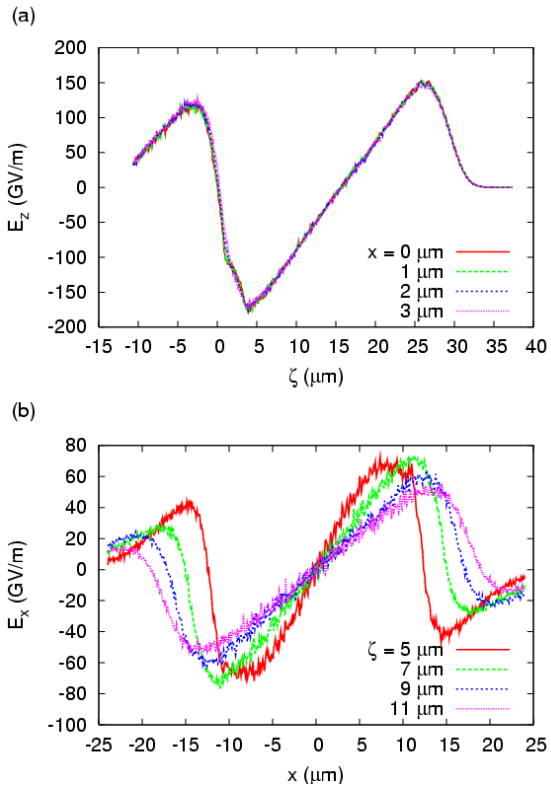

Fig. 2. (Color online) (a) Cross sectional profiles of the longitudinal electric fields are drawn at transverse positions of 0, 1, 2, and 3 μm in the z direction. The tail of the wakefield is at $\zeta = 0$. (b) Cross sectional profiles of the transverse electric fields are drawn at ζ =5, 7, 9, and 11 μm in the x direction.

E_x, at the time when the laser propagates by 96 μm. In Fig. 2(a), ζ is defined as $\zeta = z - v_p t$, where v_p is the phase velocity of the wakefield, which is the same as the velocity of the laser pulse. The tail of the wakefield is

located at $\zeta = 0$ μm. In linear regimes of wakefields, the longitudinal electric fields E_z decreases with increasing the transverse distance. However, in the blowout regime, the fields do not vary with the transverse distance [3,4], and the intensity of the fields is much higher than that in linear wakefields. In the linear wakefields, the gradient of E_x increase with increasing ζ, but it decreases with increasing ζ in the blowout regime. Also, the length of the focusing regime increases more than that of linear regimes.

The electron current generates azimuthal magnetic fields. The sign of the magnetic fields is the reverse of the sign of the transverse electric field. For a relativistic electron injected in a blowout-regime wakefield, the magnitude of the Lorentz force due to B_z fields is more than 30% of the force due to E_y fields while it is less than 15% for the linear reigme. Hence, the effect of magnetic fields on electron motion must be considered.

3. Single-particle Motion and Radiation

With the given wakefields, a single electron motion is calculated from Newton's equation of motion with Lorentz's force by using a leap-flog method for the evolution of position and velocity. The wakefields obtained with the XOOPIC code are used for the electric and the magnetic fields, assuming that the wakefields propagate with the velocity v_p in the laser propagation direction. That is to say, neither the effects of laser depletion nor diffraction are considered in this model. From the electron motion, the characteristics of the betatron radiation from the electron oscillation are also calculated using the far-field radiation theory in the time domain and the frequency domain.

III. SIMULATION RESULTS

We assume that an electron bunch is self-injected within the blowout regime. When the self-injected electrons are accelerated at the initial time, the electrons have a little higher energy than the energy corresponding to the wakefields velocity v_p, which is the same velocity of electrons with an energy of 15.3 MeV for a plasma density of $n_e = 1.93 \times 10^{18}$ cm^{-3} and a laser wavelength of $\lambda = 800$ nm. In this simulation, the injected electron is assumed to have an initial energy of 24.5 MeV.

The off-axis injected electron experiences a betatron oscillation as well as an acceleration in the longitudinal direction. In the relativistic regime, the longitudinal velocity v_z does not increase monotonously, but oscillates with a frequency that is double the frequency of the betatron oscillation. Thus, if the electron comes to have a relativistic transverse motion, the electron can have v_z less than v_p and be shifted backward in the ζ space. A

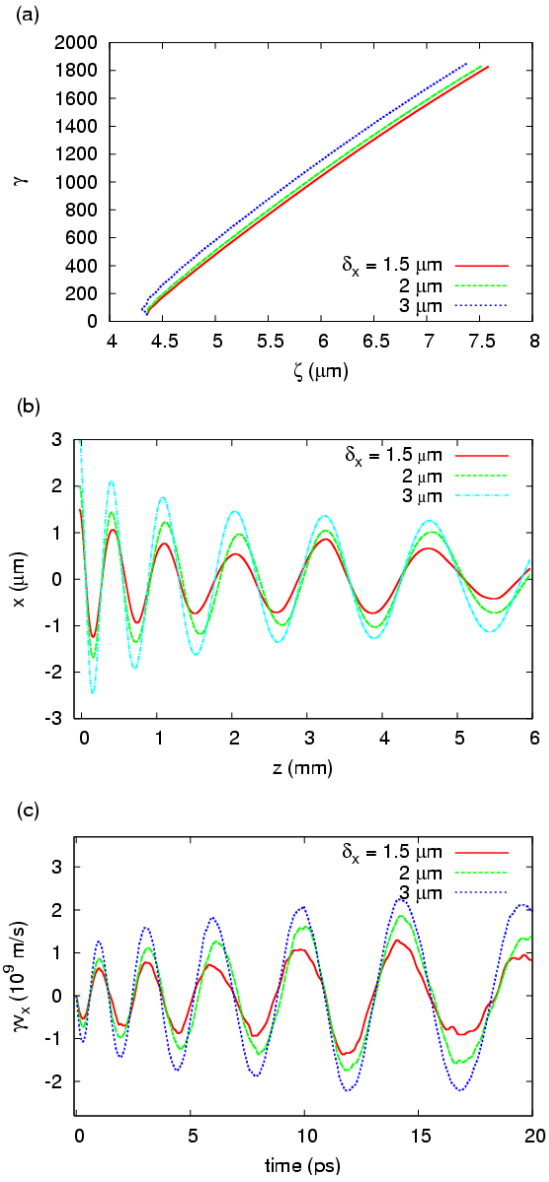

Fig. 3. (Color online) Time evolutions during 20 ps are shown for (a) the electron energy in γ-ζ phase space, (b) the electron trajectory in z-x space, and (c) the relativistic transverse velocity of the electron. An electron with an initial energy of 25 MeV is injected at $\zeta = 4.35$ and $\delta_x = 1.5$, 2, and 3 μm, respectively.

electron shifted backward experiences a higher acceleration force from the electric field and, thus, can have more energy than the electron without a transverse oscillation. Figure 3 shows the time evolution of γ, the transverse distance r, and the transverse relativistic velocity γv_z. When the transverse injection position δ_x is 3 μm, the electron slips backward for 0.5 ps, goes forward again, and reaches the maximum energy a little above $\gamma = 1800$ for 20 ps. The electron propagates with the

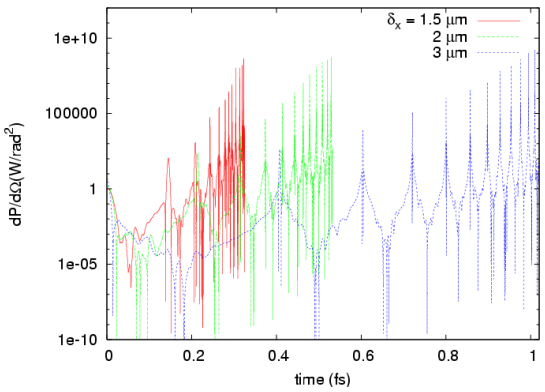

Fig. 4. (Color online) The power per radiated solid angle with time evolution. The radiation are detected in the direction of laser propagation, $\theta = 0^\circ$ and $\phi = 0^\circ$.

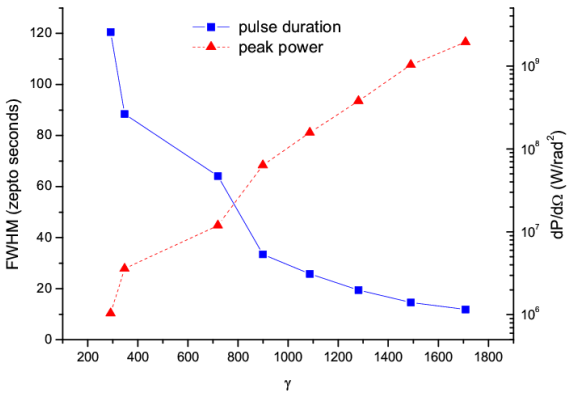

Fig. 5. (Color online) The peak power and duration of the radiation detected for each betatron radiation period. The initial injection position $\delta_x = 3$ μm and the radiation are detected in the direction of the laser propagation, $\theta = 0^\circ$ and $\phi = 0^\circ$.

oscillation of the betatron frequency defined as

$$\omega_\beta = \omega_p/\sqrt{2\gamma} \ . \tag{4}$$

E_z decreases with increasing ζ as the electron moves; thus, the gradient of acceleration decreases with the propagation. With increasing electron energy, the electron mass increases, and this causes a decrease in the betatron frequency.

The betatron radiation is emitted at the region of maximum accelerating gradients with a frequency double that of the betatron oscillation. If the radiation detector is far away from the radiation source, the detector receives each betatron radiation at a time of [12]

$$t' = t - \frac{\mathbf{n}\cdot\mathbf{r}}{c} \ , \tag{5}$$

where $\mathbf{r}$ is the position vector of the electron at the retarded time, and $\mathbf{n}$ is the normal vector in the observation direction. According to Eq. (5), the intervals of the radiations are determined by the fundamental frequency expressed as the Doppler-shifted betatron frequency [8]:

$$\omega_f = \omega_b \times (2\gamma^2) = (2/\sqrt{2})\omega_p\gamma^{3/2} \ . \tag{6}$$

The intervals decrease if the detector is in the direction of the electron propagation. However, Eq. (6) would not be applied to the betatron radiation because the electron propagation distance would be shorter than that of a electron with only longitudinal motion. Because the effect of the propagation distance contraction decreases with the transverse location δ_x, the fundamental frequency decreases slightly in the frequency spectrum domain. The total radiation time observed at the detector also increases, as shown in Fig. 4. The radiation times are 0.32, 0.53, and 1.01 fs, respectively.

The spectral radiation power is calculated as

$$\frac{dP}{d\Omega} = \frac{e^2}{4\pi c}\left|\frac{\mathbf{n}\times\{(\mathbf{n}-\vec{\beta})\times\dot{\beta}\}}{(1-\vec{\beta}\cdot\mathbf{n})^3}\right|^{\frac{5}{2}} \ . \tag{7}$$

The radiation power has three peaks, as shown in Fig. 4; one central high peak and two sideband low peaks. The central peak is related to the transverse force, and the other two low peaks are related to the acceleration of v_z. During a half betatron period, the sign of the transverse force does not change. However, when the electron reaches a peak velocity, the sign of the time derivative of β_z changes. From the view of the detector, the change in the sign occurs abruptly. The fields generating the two sidebands have signs in the opposite directions to the field generating the central peak, but the power is estimated using the square of magnitude of fields. Thus, the central peak can be observed with two low peaks beside it. As the electron energy increases, the radiation power increases, as shown in Fig. 5, and the pulse duration detected for each betatron radiation period decreases. The pulse duration is inversely proportion to the critical frequency, which is defined as [7]

$$\omega_c = (3/2\rho)\gamma^3 c = (3/2)\gamma^2|F_\perp|/mc \ , \tag{8}$$

where ρ is the bending radius of the oscillation and $F_\perp$ is a transverse force. The transverse force is almost the same during electron propagation; thus, the pulse duration is only proportional to $1/\gamma^2$.

The spectral flux emitted in the direction of observation $\mathbf{n}$ is given by [12]

$$\frac{d^2I}{d\omega\Omega} = \frac{e^2}{3\pi^2 c}\left(\frac{\omega\rho}{c}\right)^2\left(\frac{1}{\gamma^2}+\theta^2\right)^2[K^2_{2/3}(\xi) + \frac{\theta^2}{(1/\gamma^2)+\theta^2}K^2_{1/3}(\xi)], \tag{9}$$

where,

$$\xi = \frac{\omega\rho}{3c}\left(\frac{1}{\gamma^2+\theta^2}\right)^{3/2} \tag{10}$$

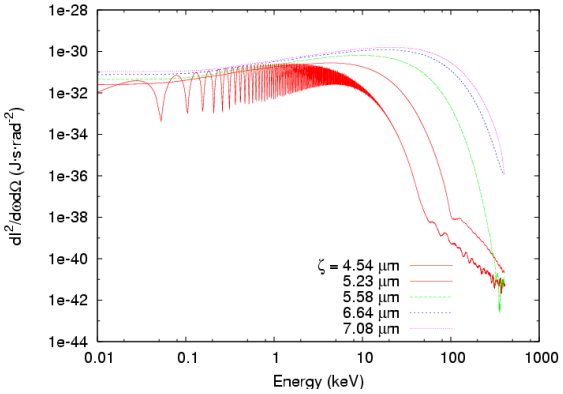

Fig. 6. (Color online) The frequency spectrum of the radiation detected for each betatron radiation period. The initial injection position $\delta_x = 3$ μm and the radiation are detected in the direction of the laser propagation, $\theta = 0^0$ and $\phi = 0^0$.

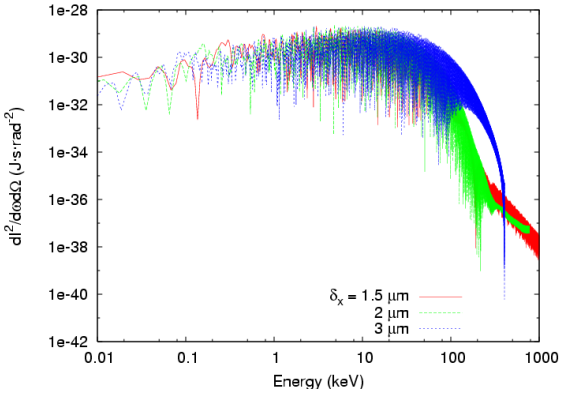

Fig. 7. (Color online) The frequency spectrum of the radiation detected during 20 ps for various transverse injection positions δ_x. The radiation is detected in the direction of the laser propagation, $\theta = 0^o$ and $\phi = 0^o$.

and K_ν is a modified Bessel function of the second kind. In the propagation direction, the spectrum increases with $\omega^{2/3}$, reaches a maximum at $0.834\omega_c$, and drops exponentially to zero above ω_c. Figure 6 shows the frequency spectrum of each radiation detected for a half period of the betatron oscillation. The peak amplitude is detected when a photon energy is 1.4, 4.27, 9.33, 17.26, or 20.92 keV, which correspond to critical energies of 1.685, 5.12, 11.91, 20.70, or 25.09 keV, respectively. Because the electron obtains more energy as it propagates, the radiation energy increases. Figure 7 shows the frequency spectrum of radiation detected for 20 ps for various transverse injection positions δ_x. The radiation is detected in the direction of laser propagation, $\theta = 0°$ and $\phi = 0°$. Equation (8) depends on the radial force. As the transverse amplitude increases, the emitted photon energy increases. The peak amplitudes are located approximately at 6, 9 and 13 keV, respectively, in Fig 7. In Fig. 6, the electron emits a peak spectral energy of around 20.92 keV at the end of propagation of $\zeta = 7.08$.

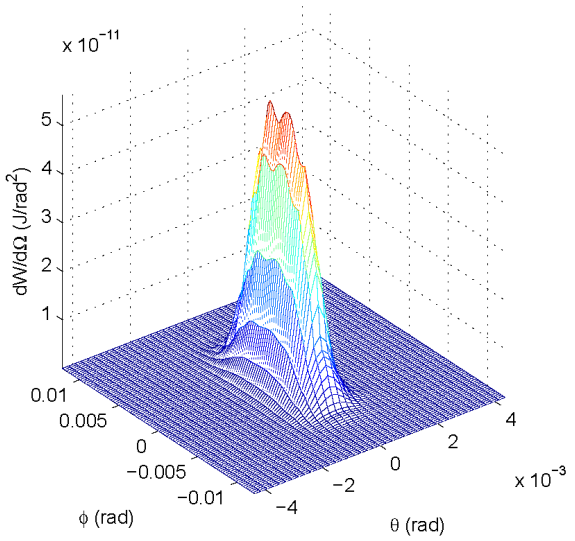

Fig. 8. (Color online) The angle distribution of the radiation power with a photon energy above 10 keV. The FWHM of the distribution is $\Delta\theta = 0.8$ mrad and $\Delta\phi = 8$ mrad.

However, the electron emits a peak energy of 13 keV in Fig. 7, which is less than 20.92 keV. The radiation energy forms a similar Gaussian distribution in the angle domain. The FWHM of the emission with a radiation energy larger than 10 keV is 0.8 mrad in θ and 8 mrad in ϕ as shown in Fig. 8. The width of the angle distribution decreases if the observer detects an energy equal to or more than 10 keV. If the detector receives any radiation above 50 keV, $\Delta\theta$ and $\Delta\phi$ becomes 0.5 mrad and 6 mrad, respectively. If the spectral flux $dI/d\Omega d\omega$ is integrated over the solid angles $d\Omega$, the spectrum of $dI/d\Omega$ is underestimated because Eq. (9) depends strongly on the observation angle.

Lastly, we simulated the radiation emitted from an electron bunch with a size of 1 μm × 2 μm injected into the axis of the blowout regime with an initial energy of 25 MeV. The tail of the bunch is located at the same injection position δ_z. We assumed that there are no repulsive forces among electrons because the space charge effect is not so strong if the total amount of charge is small and γ is large enough. The frequency spectrum of the radiation emitted from the electron bunch shows a peak amplitude is located approximately at 3 – 5 keV. This result is similar to that in a previous report [8].

IV. CONCLUSION

We demonstrated a single electron motion injected in an off-axis position of a blowout-regime wakefield. Due to the intense electric fields in the regime, the electron can be accelerated up to 900 MeV and emits an intense X-rays with an energy of 1 – 15 keV. The radiation observed in the laser propagation direction show three

peaks, two sideband low peaks and a central high peak between them. The betatron oscillation induces a decrease of the longitudinal velocity of the electron, which increases the width of the total radiation observed at the detector.

The radiation power has an angle distribution with a FWHM of 0.8 mrad in θ and 8 mrad in ϕ direction. If an observer detects a photon energy above 50 keV, the angle distribution decreases to below 0.5 mrad in θ and 6 mrad in ϕ direction. To diminish the duration of total radiation, the electron has to oscillate with a small amplitude while the electron must oscillates with a high amplitude for intense radiation power. As the electron is accelerated during the propagation, it emits high energy photons as time goes on. The energy of photons also increases with the radial amplitude of the electron motion. Lastly, from the mono-energetic electron bunch, instead of a single electron, a photon energy of 3 – 5 keV was detected. The behaviors of the spread electrons diminish the maximum photon energy, but increase the radiation intensity.

ACKNOWLEDGMENTS

This work was supported through BK21 project funded by the Korea Research Foundation and Basic Research Program.

REFERENCES

[1] W. P. Leemans, B. Nagler, A. J. Gonsalves, Cs. Toth, K. Nakamura, C. G. R. Geddes, E. Esarey, C. B. Schroeder and S. M. Hooker, Nature Physics **2**, 696 (2006).

[2] Eric Esarey and Phillip Sprangle, IEEE Trans. Plasma Sci. **24**, 252 (1996).

[3] W. Lu, C. Huang, M. Zhou, W. B. Mori and T. Katsouleas, Phys. Rev. Lett. **96**, 165002 (2006).

[4] W. Lu, M. Tzoufras C. Joshi, F. S. Tsung, W. B. Mori, J. Vieira, R. A. Fonseca and L. O. Silva, Phys. Rev. ST Accel. Beams **10**, 061301 (2007).

[5] Shuoqin Wang, C. E. Clayton, B. E. Blue, E. S. Dodd, K. A. Marsh, W. B. Mori, C. Joshi, S. Lee, P. Muggli, T. Katsouleas, F. J. Decker, M.J. Hogan, R. H. Iverson, P. Raimondi, D. Walz, R. Siemann and R. Assmann, Phys. Rev. Lett. **88**, 135004 (2002).

[6] I. Kostyukov, S. Kiselev and A. Pukhov, Phys. Plasma **10**, 4818 (2003).

[7] Antoine Rousse, Kim Ta Phuoc, Rahul Shah, Alexander Pukhov, Eric Lefebvre, Victor Malka, Sergey Kiselev, Fréderic Burgy, Jean-Philippe Rousseau, Donald Umstadter and Daniéle Hulin, Phy. Rev. Lett. **93**, 135005 (2004).

[8] Kim Ta Phuoc, Sebastien Corde, Rahul Shah, Felicie Albert, Romuald Fitour, Jean-Philippe Rousseau, Fréderic Burgy, Brigitte Mercier and Antoine Rousse, Phy. Rev. Lett. **97**, 225002 (2006).

[9] Félicie Albert, Rahul Shah, Kim Ta Phuoc, Romuald Fitour, Fréderic Burgy, Jean-Philippe Rousseau, Amar Tafzi, Denis Douillet, Thierry Lefrou and Antoine Rousse, Phys. Rev. E **77**, 056402 (2008).

[10] S. Kneip, S. R. Nagel, C. Bellei, N. Bourgeois, A. E. Dangor, A. Gopal, R. Heathcote, S. P. D. Mangles, J. R. Marques, A. Maksimchuk, P. M. Nilson, K. Ta Phuoc, S. Reed, M. Tzoufras, F. S. Tsung, L. Willingale, W. B. Mori, A. Rousse, K. Krushelnick and Z. Najmudin, Phys. Rev. Lett. **100**, 105006 (2008).

[11] J. P. Verboncoeur, A. B. Langdon and N. T. Gladd, Comp. Phys. Comm. **87**, 199 (1995).

[12] D. Jackson, *Classical Electrodynamics*, 3rd Edition (John Wiley & Sons, Inc., New York, 1999).